2.2 Vacuum

2.2.1 Introduction

Overview

This section describes the vacuum system that is part of the electron-beam transport system, including the turn-around arcs (TA and TB detailed in §2.1) connecting the two main superconducting Linacs – the north and south arcs that host the insertion devices and x-ray user beamlines – and the large turn-around arc in the existing CESR tunnel. The vacuum system includes all the chambers, pumps, gauges, valves, vacuum instrumentation and control, and vacuum facilities. The existing vacuum system of the CESR accelerator will be re-used with minimum modifications.

The vacuum chambers constitute the electron-beam delivery system that provides adequate beam aperture with low impedances for the electron beams. Adequate vacuum pumping must be installed to ensure low enough pressure so that beam loss from the residual gas scattering is not an issue for beam lifetime, accelerator component radiation damage, and radiation background to x-ray beamline user areas. From considerations of ion accumulation in the beam, gas-scattering-engendered radiation damage in the undulators, and control of beam-gas Bremsstrahlung therein, an average pressure goal of low 10^{-9} Torr range has been set.

The scope of this section is limited to the vacuum components that form the basic building blocks of the vacuum system for beam transport. There are many accelerator components that are parts of the vacuum system but serve specific functions, including beam instrumentation and control (such as beam-position monitors, beam-current monitors, x-ray-generating IDs, etc). These functional components will be described in their respective sections.

Beampipe aperture and material

In most of the beam-transport vacuum chambers, the beampipe aperture is 25 mm in the vertical and somewhat larger in the horizontal direction. In the arcs, aluminum extrusions with built-in cooling and pumping channels will be used. Efforts must be made to minimize beam impedance of the vacuum chambers, including adequate inner-surface smoothness, gentle transitions with angles less than 10° between different chamber cross-section shapes and proper RF shielding or bridging of vacuum flange joints.

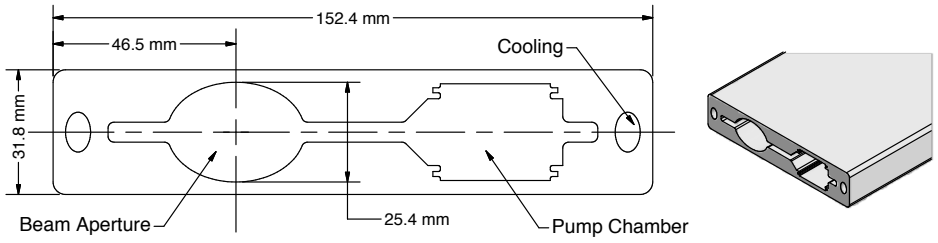

Figure 2.2.1: Extruded aluminum chambers comprise the beam aperture and the ante chamber for pumping and cooling channels.

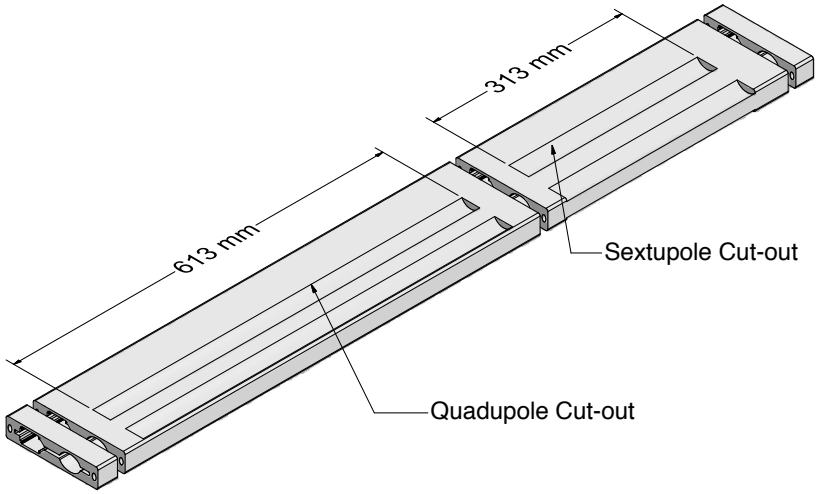

Figure 2.2.2: The extrusion with pole-tip grooves for both quadrupole and sextupole magnets

To achieve the low-thermal outgassing and the photon-induced desorption, all vacuum chambers and appendage-vacuum components will be fabricated with UHV-compatible practices, which have been well established through many years of CESR operations.

Vacuum pumping

Sufficient ultra-high vacuum-compatible pumps, both localized (lumped) and distributed, will be installed in the vacuum system to maintain the required average gas pressure (low 10^{-9} Torr range) at a beam current of 100 mA. The installed pumping system must have enough pumping speed and capacity to allow vacuum-system conditioning of reasonably short duration during the initial accelerator commissioning, and after installation of new vacuum components for upgrades and/or repairs. Typical pumps are sputter-ion pumps (noble-diode style), Non-Evaporable Getters (NEGs) and titanium-sublimation pumps (TiSPs).

Vacuum instrumentation and control

The vacuum system will be divided into sectors by RF-shielded gate valves to facilitate staged vacuum-system installations, vacuum-system upgrades, maintenance, and repairs. A typical length of a vacuum sector is 30 m.

Cold-cathode ion gauges (CCGs) will be installed periodically throughout the vacuum system to monitor vacuum-system performance and for vacuum-system trouble-shooting. Each vacuum sector will be equipped with at least one residual gas analyzer (RGA). Numerous thermocouples will monitor local temperatures of vacuum components. Monitoring and interlock functions will be integrated into the central control system.

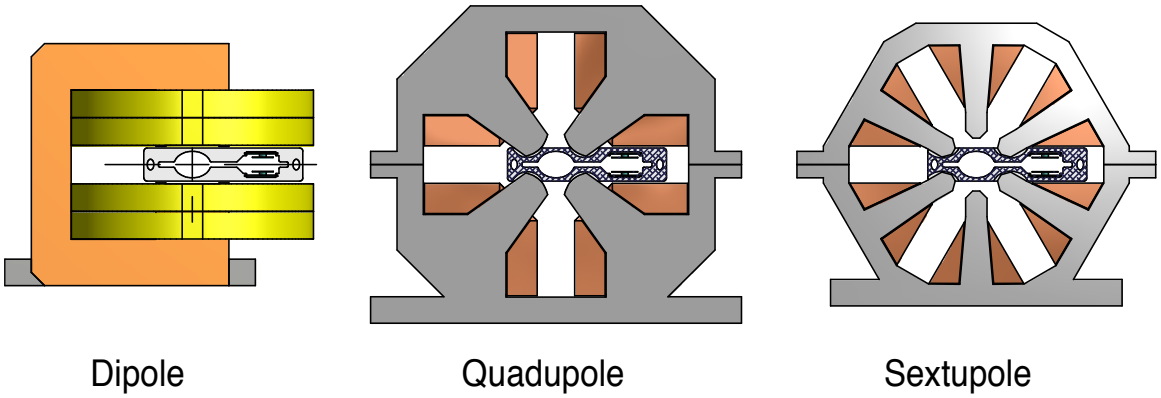

Figure 2.2.3: Cross sections of the beampipe extrusions and magnets at dipole, quadrupole and sextupole magnets.

2.2.2 Electron beam lines

Aluminum beampipe extrusions

Aluminum extrusions made of Type 6063-T4 or -T6 alloy will be employed owing to their good electrical and thermal properties, excellent machinability, and welding qualities.

The extrusion consists of a beam aperture and an ante-chamber for distributed pumps and cooling channels, as shown in Fig. 2.2.1. The pumping ante-chamber is located radially outward in the bending magnets so that synchrotron radiation generated from the bending magnets is intercepted by the water cooled walls close to the distributed pumps. This arrangement has two obvious advantages. First, it brings the distributed pumping close to the gas load from SR-induced desorption. Secondly, it significantly limits scattered photons (and photo-electrons) from entering the beam space.

Due to the short electron beam-bunch length, it is important to have the best interior surface finish possible within the beam aperture. One of the challenging requirements is to reduce surface roughness of less than 3μm rms, at least in the longitudinal dimension of the beam bore. Recent experience at LCLS proved that sub-μm rms-surface finishes are achievable [1] with a combination of high quality aluminum extrusions and further surface polishing via a technique called abrasive-flow machining [2]. The highly polished interior surfaces bring additional benefit to the vacuum system, as it reduces effective surface area, thus lowering the static thermal-outgassing rate. Such finishes have been achieved during careful extrusion [3].

Aluminum beampipe extrusions in magnets

The aluminum extrusion shown in Fig. 2.2.2 will be used for most of the vacuum chambers passing through magnets. In the dipoles, the extrusion will be bent to the required radius. In quadrupole and sextupole magnets, grooving, as illustrated in Fig. 2.2.2, will be done to bring the magnet pole tips as close to the electron beam as possible, while maintaining sufficiently strong structure for withstanding atmospheric pressure. Figure 2.2.3 shows cross-section views of the extrusion in magnets.

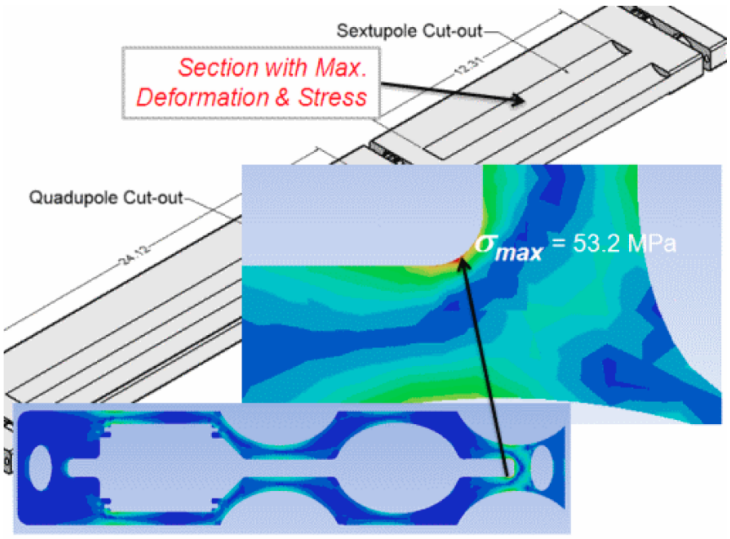

Figure 2.2.4: Calculated deformation of the chamber extrusion after pole-tip grooving. Maximum deformation is ≈ 0.1 mm in the middle of a sextupole magnet, and maximum stress at the corner is ≈ 53.2 MPa, well below material yield stress of 240 MPa for 6063-T6 aluminum alloy

The mechanical stress and deformation caused by atmospheric pressure on the extrusions was evaluated using the commercially available mechanical-design and simulation code ANSYS®. As expected, maximum deformation and stress occurs at locations where the maximum amount of material is removed, in the center of a sextupole magnet. The calculated maximum deformation and stress are 0.10 mm and 53 MPa, respectively, (as shown in Fig. 2.2.4). The calculated maximum stress is well below the yield stress (≈ 240 MPa) of Type 6063-T6 aluminum alloy.

Conceptual vacuum chamber design

Building blocks are attached to the aluminum extrusions, via TIG welding, to form various functional vacuum chambers. The building blocks must be fabricated with UHV-compatible materials. Due to the nature of very short electron-bunch length, it is important to avoid steps and gaps on the interior wall in the vicinity of the electron beam with dimensions comparable to the bunch length. When a beam aperture cross-section change is necessary, a smooth transition must be used, keeping the inclination angle less than 10° with respect to the electron beam.

Some conceptual vacuum chambers with functional components are shown in Fig. 2.2.5 to Fig. 2.2.9. As depicted in Fig. 2.2.5, NEG strips mounted on hangers are inserted in the ante-chamber to provide distributed-vacuum pumping. The NEG strips are electrically insulated from the chambers, so they may be resistively heated during activation. For initial pumpdown and NEG activation, localized pumps, typically sputter-ion pumps, are connected to pump ports, as illustrated in Fig. 2.2.6. To facilitate fabrication and installation, UHV

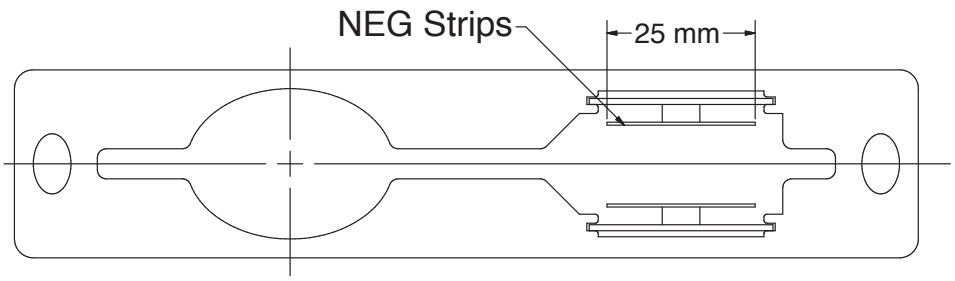

Figure 2.2.5: NEG strips are mounted in the ante-chamber, located on the radial outside of a bending magnet, close to the SR-induced gas load.

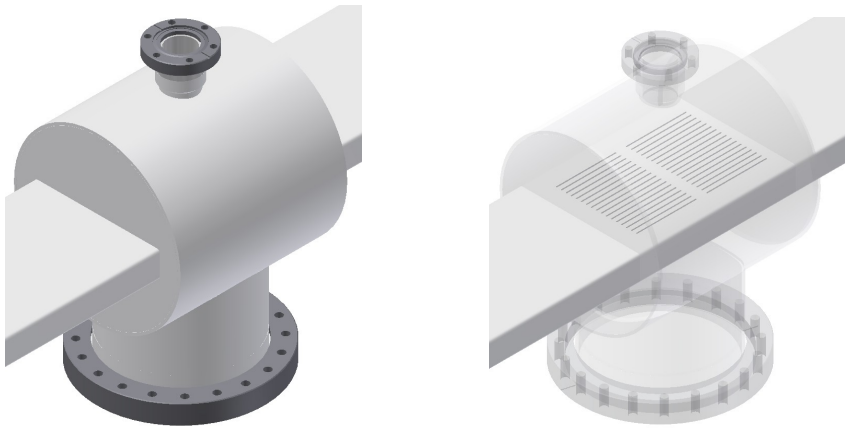

(a) (b)

Figure 2.2.6: Lumped pumps are installed at pump ports comprising a shroud (Fig. 2.2.6a) welded around the extrusion with pumping slots and (Fig. 2.2.6b) cutting through both top and bottom.

flanges (ConFlat®-type) with metallic seals are attached to the ends of vacuum chambers, with an example shown in Fig. 2.2.7. Explosion-bonded aluminum to stainless-steel-transition blocks are used not only to facilitate welding, but also to provide a smooth cross-section transition from the complex extrusion cross section to a simple rectangular one. The rectangular cross sections at the flanges are desirable for joining the chamber to many essential vacuum components, such as RF shielded bellows and RF-shielded UHV gate valves.

A conceptual vacuum chamber is shown in Fig. 2.2.8 with integrated components. Integration of the chamber into an accelerator period in the south arc is given in Fig. 2.2.9.

Synchrotron radiation power

To assess vacuum-chamber cooling requirements, synchrotron-radiation (SR) power density on the vacuum chambers was calculated for 100 mA electron beam at 5 GeV. SR radiation only from bending magnets is considered as SR from the insertion devices will be extracted to the user beamlines. For simplicity, the SR calculation was done for a uniform beampipe of

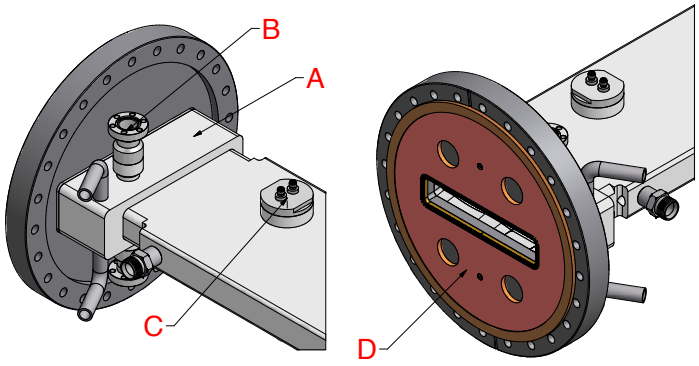

Figure 2.2.7: Conceptual vacuum chamber design. Stainless-steel (SST) UHV flanges are welded to the Al extrusions via explosion bonded SST/Al transitions (A). The transition also hosts a pair of ports (B) for electrical connections to the NEG strips. An RF-insert gasket with beryllium-copper finger contacts (D), is used to bridge the gap in the flange joint. The beam-position monitor (BPM) assembly, (C), is directly welded to the extrusion.

25.4 mm inner diameter (ID) throughout the electron-beam line. In practice, the beampipe IDs that intercept SR are always equal or larger than 25.4 mm, thus the actual SR power-area density will be generally lower than calculated here.

The calculated SR linear-power and area-power densities on the vacuum chamber walls are shown in Fig. 2.2.10. On average, the SR power deposited on the vacuum-chamber walls is $\approx 100\,\mathrm{W/m}$. With a typical chamber cooling loop of $\lesssim 10$ m in length, a cooling-water flow rate of 0.5 GPM is sufficient to keep the average chamber temperature rise less than 10° C. The thermal stress of the aluminum chamber, induced by the vertically narrow SR strip, is calculated for a maximum power density of $3\,\mathrm{W/mm^2}$. The result, shown in Fig. 2.2.11, indicates the thermal stress is well below the yield stress of the material with adequate cooling.

Vacuum pumping and pressure distributions

The pressure profiles are calculated in the electron beamlines, using a 1D finite-element method developed at CESR, in which the electron-beam transfer lines are divided into 10 cm segments. The purpose of the calculation is to provide a general assessment of the conceptual vacuum design. Many special beamline components (such as in-vacuum insertion devices and electron-beam collimators) are not considered.

Two sources of gas load are included in the calculations: the thermal desorption and the SR-induced desorption from the vacuum chamber walls. A thermal outgassing rate of 10^{-11} Torr $\times$ liter/s/cm^2 (at room temperature) is used to calculate the thermal gas-load. The SR-induced gas-load is calculated using the SR photon flux (F_{SR}, see Fig. 2.2.12),

$$\dot{Q} = \eta_{\mathrm{ph}} \cdot F_{\mathrm{SR}} \tag{2.2.1}$$

with a photon desorption yield η_{ph} (molecules/photon). With properly cleaned vacuum cham-

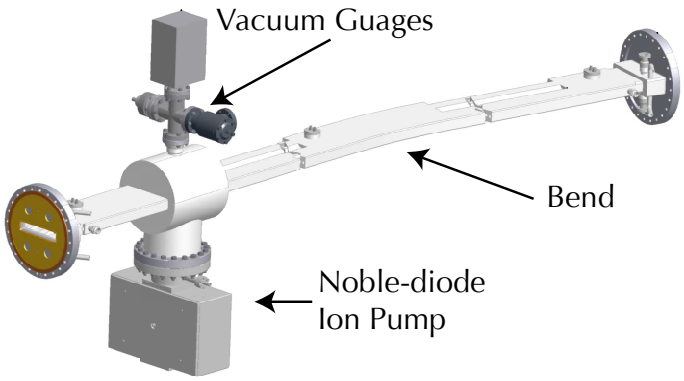

Figure 2.2.8: A vacuum chamber with integrated vacuum pumps, gauges, BPMs and features to accommodate dipole, quadrupole and sextupole magnets.

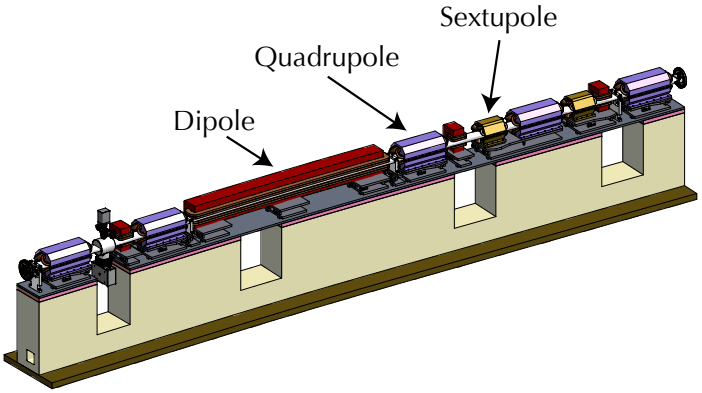

Figure 2.2.9: A typical period in the South Arc.

bers, the SR desorption yield decreases with beam dose, typically following

$$\eta_{\rm ph} \propto D^{-\alpha} \tag{2.2.2}$$

where D is the accumulated electron-beam dose (in Ampere-hour), and $\alpha = 0.6 \sim 1.0$. Operational experiences showed that the SR-desorption yield drops below 10^{-6} molecule/photon after accumulation of a few 100 Ampere-hour, as demonstrated from CESR operational experience (see Fig. 2.2.13).

Adequate vacuum pumping needs to be installed to achieve the required vacuum level, that is, with average pressure in the low 10^{-9} Torr range. Though the final vacuum-pumping configuration is yet to be developed, a model of evenly spaced pumps is used for this calculation, with an exception in the CESR portion of the electron-beam line, where existing lumped and distributed-ion pumps are used in the calculations. Two categories of vacuum pumps are used: localized pumps (or lumped pumps, LPs) and distributed pumps (DPs). The LPs are mounted on pumping ports (see, for example, Fig. 2.2.6), and they may be noble diode sputter-ion pumps, cartridge NEGs or TiSPs. The LPs will be the primary pumps for the initial vacuum-system pump-down and beam conditioning. The DPs are mounted in the ante-

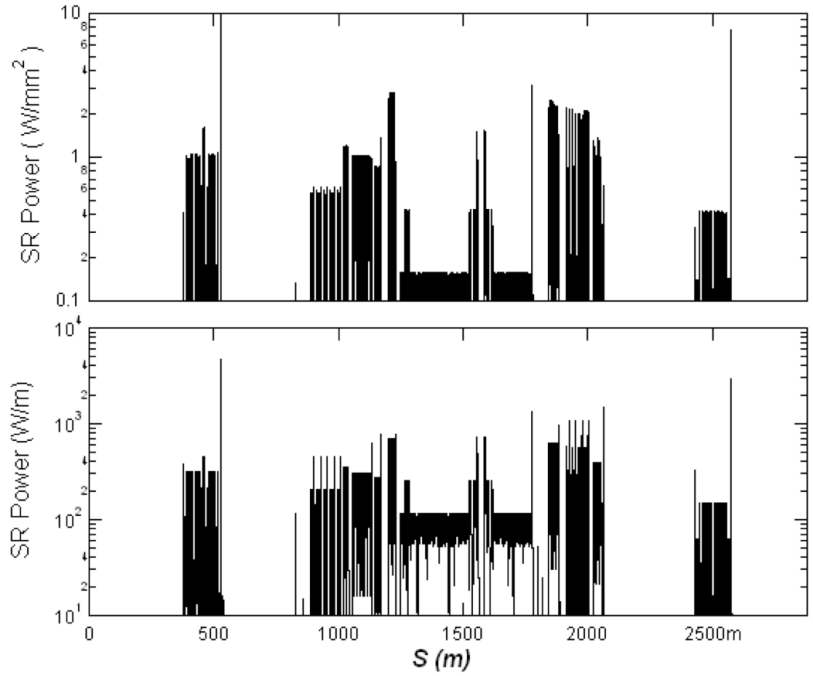

Figure 2.2.10: Calculated synchrotron radiation (SR) linear-power and area-power densities on the walls of the vacuum chambers, for 100 mA electron-beam current at 5 GeV. All calculations are done with uniform beam pipes of 25.4 mm inner diameter. (The exceptions are at the entrance of the Linacs, located at ≈ 500 m and ≈ 2500 m, where actual beampipe-aperture changes are taken into account. These result in spikes in the calculated power level at these locations.)

chambers of the beam chambers. In the CESR section, existing distributed-ion pumps will be re-used. In the other sections, NEG strips (st707 type by SAES Getters Inc.) will be used (see, Fig. 2.2.5). The typical pumping speed for the LPs and DPs are listed in Tab. 2.2.1 for all sections, excluding the superconducting Linacs. The pumping speed of the NEG strips may decrease due to saturation [4]. The calculated pressure profiles at various NEG conditions are shown in Fig. 2.2.14. The results clearly indicate that the proposed vacuum-pumping installation is able to maintain the average pressure well, even with partially saturated NEG strips in the accelerator parts TA, NA, SA and TB that have been designed in §2.1.

To maintain effective pumping, the distributed NEG strips need to be re-activated before significant saturation. However, the NEG activation process requires significant downtime (on the order of eight hours or longer) due to hydrogen outgassing during the activation and the pressure recovery following the activation. In Tab. 2.2.2, the NEG-strip-time duration between activations is estimated for TA, NA, SA and TB sections. For well-conditioned vacuum chambers, the residual gas is usually composed >90% of H_2, and <10% of CO, CH_4, H_2O, CO_2 in combination. It is well-known that NEG has extremely high pumping capacity for H_2 so the NEG saturation is normally due to adsorption of carbon- and oxygen-containing molecules. Correspondingly, the gas-load listed in the Tab. 2.2.2 represents 10% of the amount

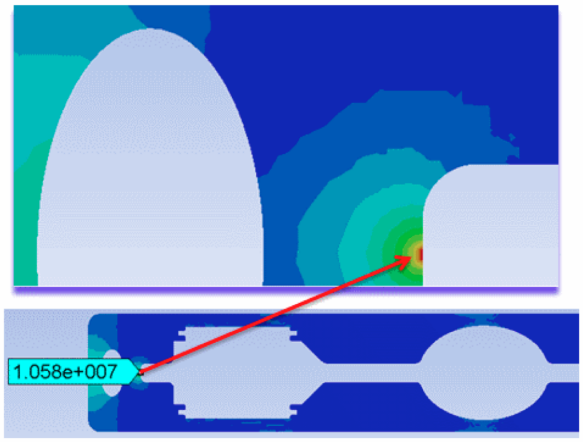

Figure 2.2.11: ANSYS calculation shows the thermal stress at locations with maximum SR power density ($3\,\mathrm{W/mm^2}$) is $\approx 10.6\,\mathrm{MPa}$, well below the yield stress (240 MPa) of 6063-T6 aluminum alloy. A film coefficient of $1000\,\mathrm{W/m^2/K}$ at the cooling surface was used for the calculation.

of SR-induced gas-load as calculated by Eq. (2.2.1), using data reported in [4]. The calculations clearly indicate that the installed NEG-pumping capacity is sufficient, and the activations may easily fit in the scheduled accelerator maintenance downtime.

2.2.3 X-ray frontend and transport

X-ray frontend design

Insertion devices in the North and South Arcs generate high-brilliance SR radiation for the x-ray users. Special vacuum components, referred to as the x-ray frontend, are used to safely separate the x-ray beams from the electron beam. The x-ray frontend allows operational independence between the accelerator and the x-ray user systems. The frontends are gener-

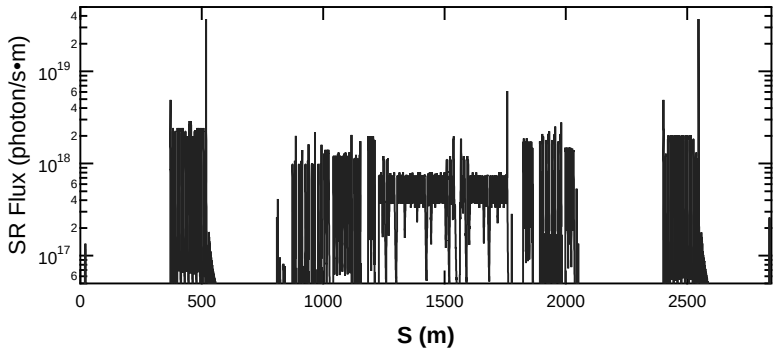

Figure 2.2.12: Calculated total SR photon flux impinging on both inner and outer walls of the beam pipes with uniform 25.4 mm aperture.

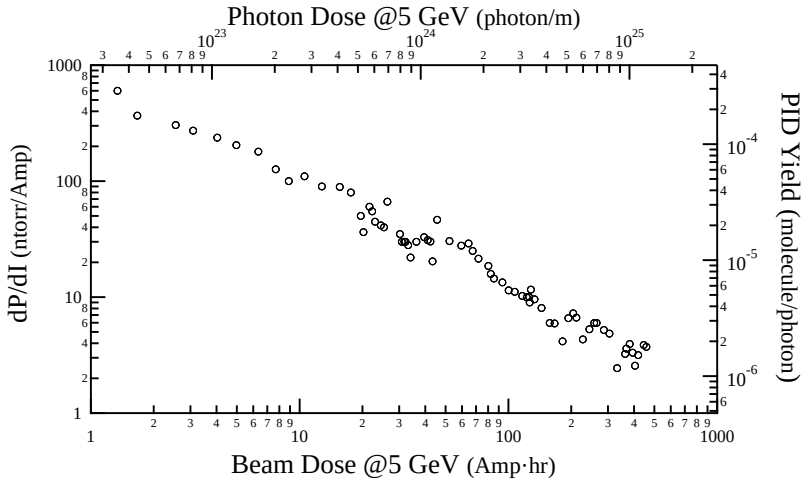

Figure 2.2.13: A typical vacuum-beam conditioning trend of a newly installed aluminum chamber in a CESR dipole magnet.

Table 2.2.1: Installed pumping speed along electron-beam transfer lines. Notes: A) NEG pumping speed for N_2 at full activation, see [4], B) Distributed ion pump in CESR was measured for N_2

section	LP speed (l/s), every 3 m	DP speed (l/s/m)	Note
TA	40	350	A
SA	40	350	A
CE	100	100	B
NA	40	350	A
TB	40	350	A

ally located on the accelerator side of the facility (as defined by radiation shield wall). The frontends are installed at the same time as the electron beam line components, allowing later development of the x-ray lines as needed.

Figure 2.2.15 shows the beam line frontend of G-line at CHESS, which may serve as a model for ERL beamlines. A 'crotch' provides a safe branch off of the electron beam and the photon beam. A pair of UHV-gate valves and a pair of photon shutters allow independent operations of the accelerator and the beamline-user facility.

Crotch

The power density of the SR (primarily originating from an adjacent bending magnet) striking the crotch, or junction between the x-ray beamline and the main electron beamline, can be very high. Careful design of the vacuum surface and cooling channels is required. Two types of design are presented here.

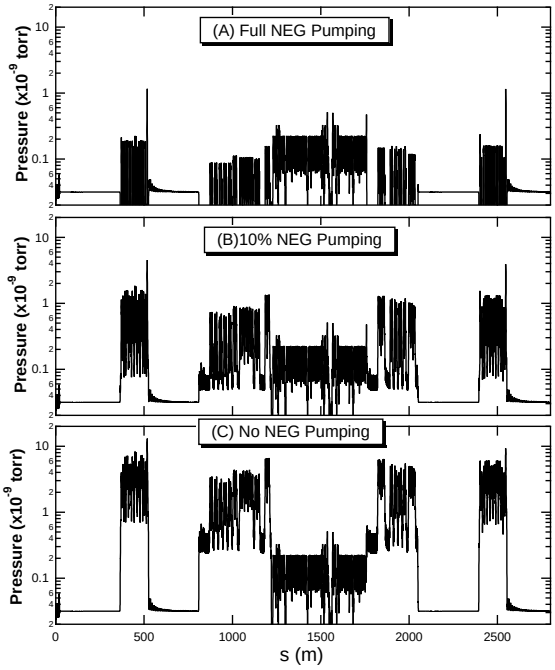

Figure 2.2.14: Calculated pressure profiles along the beam pipe for a 100 mA electron beam at 5 GeV, with desorption yield $\eta_{\rm ph} = 10^{-6}$ molecule/photon, at various NEG pumping speeds.

Figure 2.2.16 shows a crotch used at the CHESS G-line. This is a fully flanged chamber that is directly inserted into the main accelerator beamline. The crotch assembly is constructed from OFHC copper, with a gently inclined surface intercepting the SR fan from a bending magnet (of 87 m bending radius). The water-cooled inclined surface was designed for a 500 mA electron beam at 5 GeV, significantly above the total power requirement for the ERL beamlines. Thus a scaled-down design may be suitable.

Figure 2.2.17 shows a more compact crotch design, which is used at APS and NSLS II. The compact design allows the absorber to be inserted in a side port on a dipole chamber where an x-ray beamline branches off. To handle a much higher power density, the absorbers are made of Glidcop®(copper-based metal-matrix composite alloys mixed primarily with aluminum-oxide ceramic particles).

Photon shutter

As seen in Fig. 2.2.18, photon shutters are used to stop the intense SR beam generated by the IDs, allowing radiation isolation between the main accelerator vacuum and the x-ray beamline users. Adequate thermal design must be implemented to handle very high power density. Figure 2.2.18 shows a model design of a photon shutter used in the CHESS G-line frontend. An engineering design is needed for the Cornell ERL, as the x-ray beam power density of the ERL IDs will be significantly higher than that of the CHESS G-line. Normally, a pair of photon shutters is installed in a series for additional operational safety.

Table 2.2.2: NEG Duration with continuous 100 mA Operation

Section	Average SR Flux (Photon/s/m)	SR Gas-load (CO-equivalent) (Torr×l/s/m)	Time before losing 50% pumping speed (Days at 100mA)
TA	7.80×10^{16}	2.21×10^{-10}	89
SA	3.42×10^{16}	9.68×10^{-11}	203
NA	3.91×10^{16}	1.11×10^{-10}	178
TB	6.49×10^{16}	1.84×10^{-10}	107

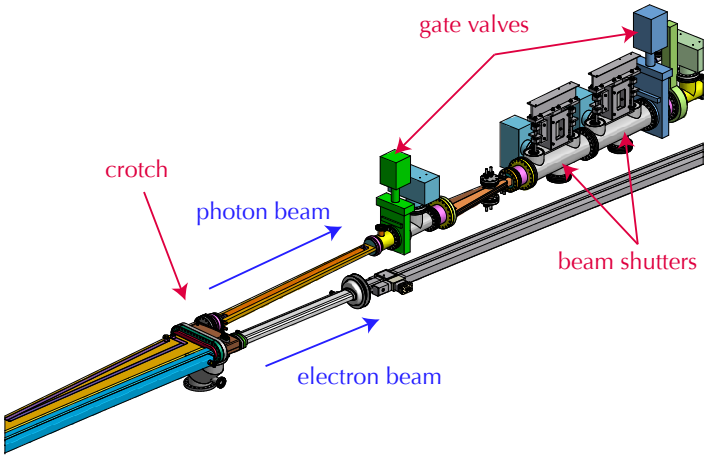

Figure 2.2.15: CHESS G-line frontend as a design model. The x-ray beamline physically separates from the electron-beam line at the crotch. In normal operation, the x-rays generated from an ID may reach the users with the gate valves and the photon beam stops open. When not needed, the photon shutters safely absorb the x-rays while not affecting the operation of the accelerator.

2.2.4 Special vacuum components

In-vacuum IDs

In-vacuum insertion devices (IV-IDs) are used to produce the high quality x-ray beams. As a complex system, an IV-ID should be designed as a self-contained device, with its own vacuum pumping and instrumentation. The detailed description of the IV-IDs is given in §2.7.

Protector for IDs

For the longevity of small-bore IV-IDs, an electron-beam collimator or protector is used at the entrance of every IV-ID to protect it from synchrotron radiation and particles lost through IBS and gas scattering. A conceptual protector design is presented in Fig. 2.2.19, comprising a copper vacuum beampipe and an iron-radiation shield. For optimal radiation shielding, a high-Z material (tantalum) lining is inserted in the copper beampipe. The radiation-shielding

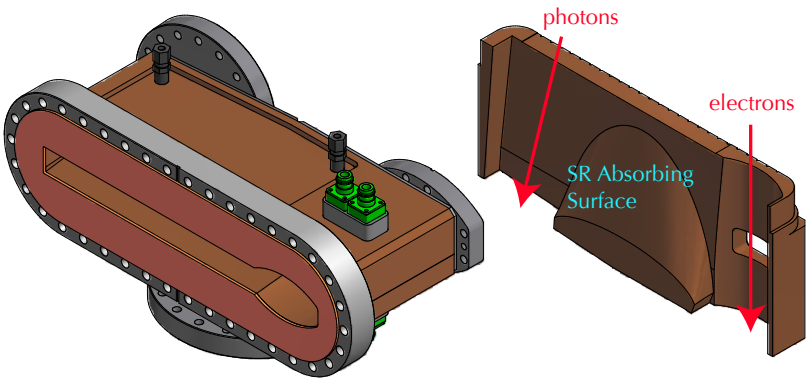

Figure 2.2.16: Crotch design for CHESS G-line (left) with a water-cooled top half (right). The inclined-vacuum surface on the top half stops SR fan from the upstream bending magnet.

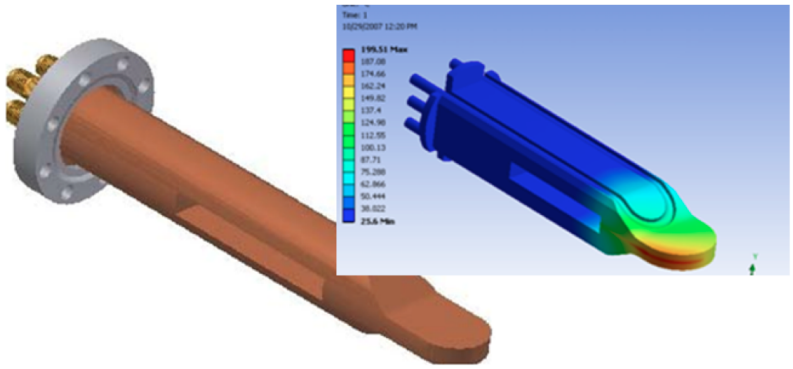

Figure 2.2.17: NSLS II insertable crotch design. To handle very high SR power density, the heat absorber is made of Glidcop®.

considerations of the protector design is described in §2.1.17. Vacuum aspects of the protector are presented here.

Copper is chosen as the beampipe material, to provide better a radiation-shielding effect in the forward direction as compared to aluminum. A taper at the entrance of the collimator, with full opening angle of 10°, provides a beam-aperture transition from a 25 mm to 5 mm diameter, the aperture of a typical IV-ID. The water-cooled taper will shield the IV-ID from any SR, up to a few hundred watts. The expected electron-beam loss along the beampipe is well below 10^{-10} A, with a power deposition of less than 1 W; thus additional cooling for the center portion of the beam pipe is not needed. The taper is welded to a 1 m-long copper tube with a thick wall (25.4 mm OD, 5.0 mm ID), going through the radiation shields of the collimator.

A water-cooled aluminum taper assembly is used to provide smooth transition in the horizontal walls between an extruded-aluminum chamber and the protector. A concept for such a taper assembly is given in Fig. 2.2.20.

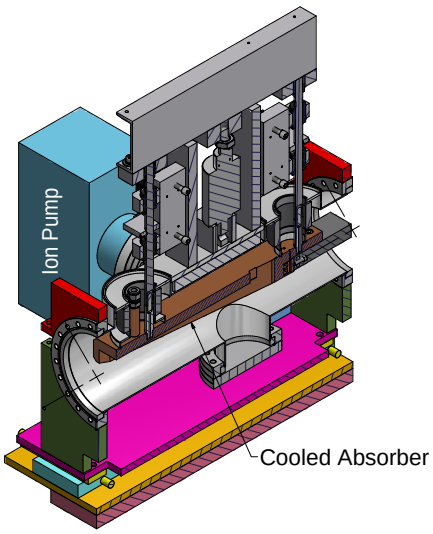

Figure 2.2.18: Beam shutter used at CHESS G-line. It is capable of absorbing a full photon beam generated from a G-line wiggler with 500 mA electron-beam current at 5 GeV.

Electron beam collimators

There are electron-beam losses along the electron-beam lines due to IBS. Electron-beam collimators are installed in the electron-beam transport lines at strategic locations (based on beam-lattice design and the accelerator's physical layout, see §2.1.17) to 'clean' up the electron beam. A concept for the collimator is given in Fig. 2.2.21. At some locations, the collimator may intercept up to a 163 nA beam-loss current, dumping 800 W power onto the first half of the center aluminum-beam pipe. Thus water cooling is also needed for the center aluminum-beam pipe.

Unlike the ID protectors, it is required to transition the beam-pipe aperture between the 5 mm ID and the extruded beampipe down stream. A pair of transition tapers, as shown in Fig. 2.2.20, will be used on both ends of the collimator.

Beam position monitors

Beam position monitors (BPMs) are essential for the electron-beam transport lines. Two types of BPMs will be considered, as depicted in the conceptual designs of Fig. 2.2.22. An engineering design will have to consider detailed issues like impedance matching and fabrication. Pickup buttons are the most commonly used and can be readily deployed directly on the aluminum extrusion with minimum space requirement. In the button-type design, the BPM assembly may be 'mass-produced' economically. The pickup buttons are welded to the coaxial vacuum feedthroughs (SMA-type), which are in turn welded onto housing blocks made of explosion-bonded aluminum-to-stainless-steel transitions. The stripline BPMs are more sensitive, as compared to the pickup buttons. Stripline BPMs, as shown in Fig. 2.2.22b, were successfully fabricated at Cornell and installed at the prototype ERL injector. However, the stripline

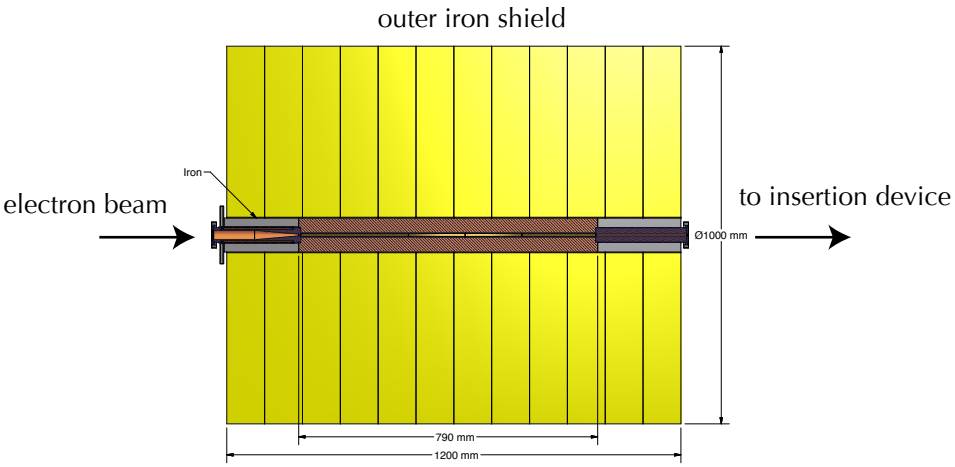

(a)

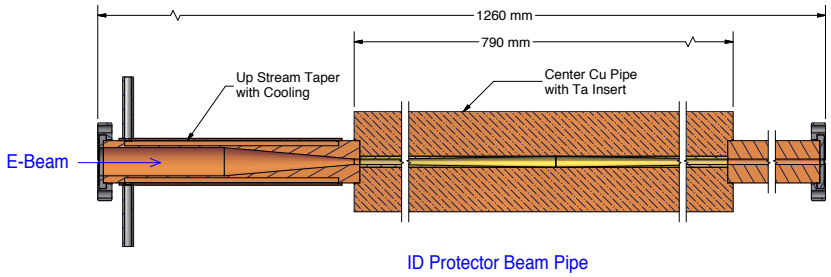

(b)

Figure 2.2.19: A conceptual design of the protector for small-bore in-vacuum ID. Figure 2.2.19a shows a protector with a copper vacuum beampipe and iron radiation shield; Figure 2.2.19b shows the copper vacuum beampipe with water-cooled up-stream taper from 25 mm to 5 mm beam aperture, and tantalum inserts.

BPMs are much more costly and more difficult in fabrication. These BPMs normally need to be fully flanged (due to the required tuning procedure) and also require beam-aperture transitions; thus they demand significantly more space.

Ion-clearing electrodes

Residual gas in the beampipe is readily ionized, predominantly by collisions with the high-energy electron beam. Positive ions are attracted to electron beams and create a nonlinear potential in the vicinity of the beam, which can lead to beam halo, particle loss, optical errors, or transverse and longitudinal instabilities. The ion-trapping and its impact to the electron beam in the ERL was analyzed in [5]. As discussed in that paper, the neutralization time for a residual gas by electron-beam collision can be calculated as

$$\tau_{\mathrm{col}} = (\sigma_{\mathrm{col}} \cdot \rho_{\mathrm{gas}} \cdot c)^{-1} \tag{2.2.3}$$

where σ_{col} is the collision-ionization cross section, ρ_{gas} is the gas density, and c the speed of light in vacuum. The neutralization times are calculated for a pressure of 10^{-9} Torr, with a gas

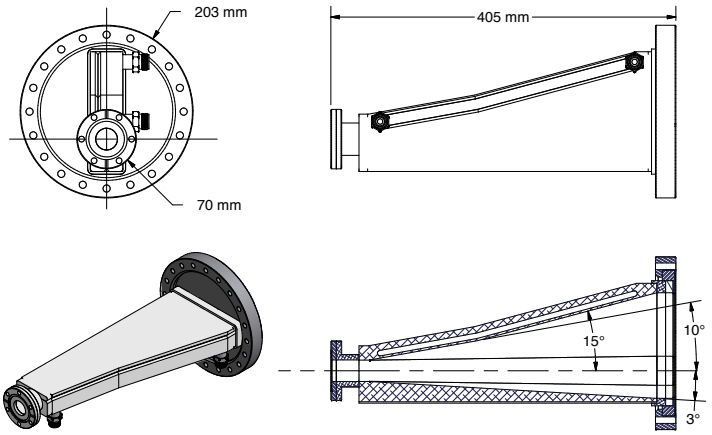

Figure 2.2.20: Transition taper is used to connect an aluminum vacuum chamber to a collimator.

Table 2.2.3: Neutralization time for dominant gases in ERL

Gas	$\sigma_{\rm col}$ ($\rm m^2$)	$\rho_{\rm gas}$ ($\rm m^{-3}$)	$\tau_{\rm col}$ (s)
H_2	3.1×10^{-23}	3.0×10^{13}	3.6
CO	1.9×10^{-22}	3.5×10^{12}	5.0
CH_4	2.0×10^{-22}	1.8×10^{12}	9.5

composition of 85% H_2, 10% CO and 5% CH_4, as listed in Tab. 2.2.3, which clearly indicate that the ions can be readily trapped in the ERL beam.

In many electron accelerators (such as electron storage rings), the trapped ions may be cleared simply with a sufficiently long gap between electron bunches. However, the clearing gap can introduce an undesirable transient in the superconducting-RF Linac. Therefore, ions have to be cleared from the electron-beam region by some other means. The only tested approaches are electro-static clearing electrodes. The clearing electrode must create an electric field at the center of the electron beam that is stronger than the beam field exerted on the ions. The calculation [5] shows that the required clearing field may be as high as 150 kV/m. With a pair of DC electrodes on top and bottom of the beampipe of a 25 mm vertical aperture, a clearing DC-voltage of ±1.9 kV is needed. To enhance the effectiveness of the clearing, the electrodes are placed at the locations of beam-potential minima.

In the clearing electrode design, it is critically important to minimize beam impedance introduced by the electrodes and to avoid significant RF excitations in the gaps behind the electrodes (that are necessary for withstanding required DC voltages). In a recent development for the large storage rings of the KEK B-factory[6] and at Cornell's CesrTA accelerator project [7, 8], low-profile clearing electrodes are developed as a electron-cloud suppression technique. These electrodes are directly deposited onto the vacuum-chamber wall via thermal-spray technology. Figure 2.2.23 depicts such an electrode implemented at the bottom of vacuum beampipe in a superconducting wiggler of CesrTA. The thickness of both the dielectric coating (Al_2O_3) and the metallic coating (tungsten) is ≈ 0.20 mm, which is proven to

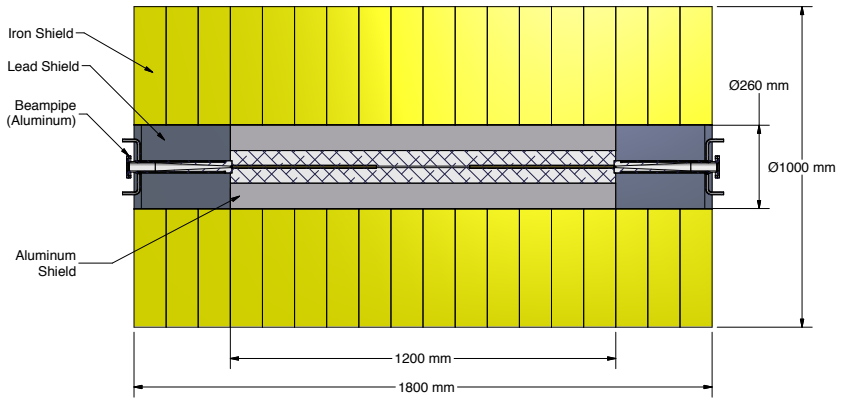

(a)

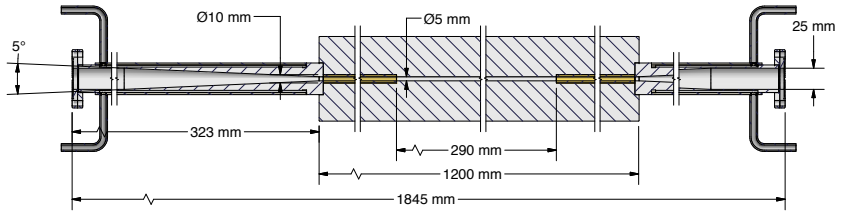

(b)

Figure 2.2.21: A conceptual design of electron beam collimator. Figure 2.2.21a shows a collimator with a aluminum vacuum beampipe and iron radiation shield; Figure 2.2.21b shows the aluminum vacuum beampipe with water-cooled up-stream taper from 25 mm to 5 mm beam aperture and tantalum inserts. Tantalum sleeves are inserted in the center aluminum beampipe for more effective radiation shielding.

withstand DC voltages up to 2 kV, meeting the required ion-clearing voltage for ERL. Means for absorbing the deposited beam-wake energy need to be devised.

RF shielded bellows

Flexible bellows with proper RF shielding are required periodically in the electron-transport beamline to allow for thermal expansion and contraction during accelerator operations and to facilitate beamline component installation and replacement. Two conceptual designs are considered here, as shown in Fig. 2.2.24. Design A is similar to the RF-shielded bellows currently used in the CESR, with beryllium copper contact springs travelling with the 'male' sliding flange. Design B is derived from a DAΦNE design [9], with 'floating' RF contacts. The pros and cons of these two designs are compared in Tab. 2.2.4. The designs shown here are fully flanged. In practice, the sliding joint assembly may be directly welded to the beampipe without flange(s), not only to minimize required space, but also to reduce beam impedance associated with flange joint(s).

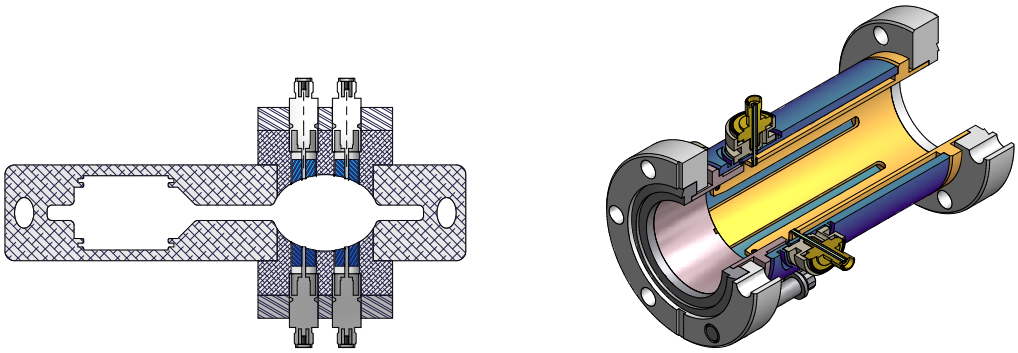

(a) BPM design A (b) BPM design B

Figure 2.2.22: Two types of BPM designs are to be considered: (A) pickup buttons and (B) striplines.

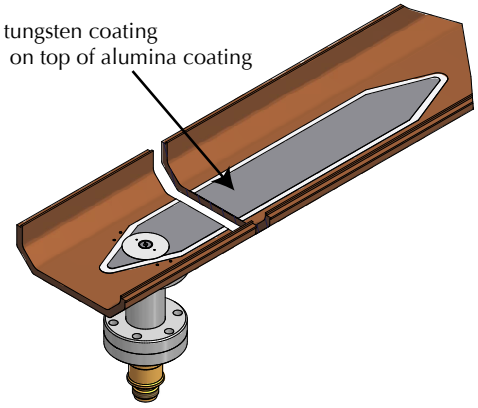

Figure 2.2.23: Electrode deposited on the vacuum chamber via thermal-spray technology. The electrode has already been used for electron clearing in a superconducting wiggler as a part of CesrTA project.

2.2.5 Vacuum system procurement

Procurement for the vacuum system is discussed in the Project Execution Plan [10]. Some vacuum chambers and components will be built in house; most however will be fabricated by qualified vendors, using CLASSE designs. These include dipole- and multipole-extruded aluminum chambers, IDs (both in-vacuum and ex-vacuum), UHV-pumping chambers and pumps, RF-shielded bellows, RF-shielded gate valves, BPMs and crotches. CLASSE personnel will work closely with the vendors in drafting fabrication specifications and procedures.

On-site vacuum facilities and associated personnel are described in [10] and are necessary to perform the following tasks:

- Acceptance of all vacuum chambers and components
- Final cleaning (particulates)

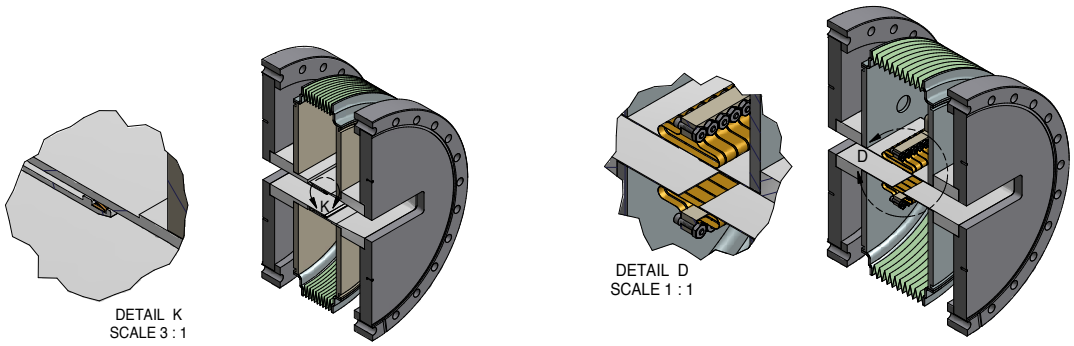

(a) Design A (b) Design B

Figure 2.2.24: Conceptual designs for RF-shielded bellows.

Table 2.2.4: Comparison of two RF-shielded bellows

Style	Pros	Cons
CESR	Simple design Unlimited stroke Local experience	Larger vertical step ($\lesssim 2\,\mathrm{mm}$)
DAΦNE	Low impedance Angular flexibility	Many small parts Limited stroke

- Final assembly onto girders and alignment
- Vacuum bakeout prior to installation
- On-site repair and modification
- Fabrication (including proto-type) of unique vacuum components
- Vacuum equipment staging and maintenance

Space for these facilities is housed in the existing Wilson laboratory, in close-by rented areas, or designed into the architectural plans developed by ARUP [11].

References

[1] Trakhtenberg, E., *et al.* *LCLS Extruded Aluminum Chamber - New Approaches.* In *Proceeding of MEDSI/Pan-American SRI2008 Workshop.* Saskatoon, Saskatchewan, Canada (2008). http://www.lightsource.ca/medsi-sri2008/pdf/PPT-LCLS_extruded_aluminum_vacuum_chambers.pdf.

[2] Benedict, G. F. *Nontraditional manufacturing processes.* CRC Press (1987).

[3] *Budgetary Estimate for ERL Beamline Components.* Technical Report report 3086-BP-8384-0, Research Intruments (2010). Report is on file at Cornell.

[4] Benvenuti, C. and P. Chiggiato. *Pumping characteristics of the St707 nonevaporable getter (Zr 70 V 24.6-Fe 5.4 wt %).* Journal of Vacuum Science & Technology A: Vacuum, Surfaces, and Films, **14** (6), pages 3278–3282 (1996). doi:10.1116/1.580226.

[5] Hoffstaetter, G. H. and M. Liepe. *Ion clearing in an ERL.* Nucl. Instr. and Meth. A, **557** (1), pages 205–212 (2006).

[6] Suetsugu, Y., *et al.* *Demonstration of electron slearing effect by means of a clearing electrode in high-intensity position ring.* Nucl. Instr. and Meth. A, **598** (2), pages 372–378 (2009).

[7] Palmer, M. A. *et al.* *Electron Cloud at Low Emmittance in CesrTA.* In *Proceedings of the first International Particle Accelerator Conference*, pages 1251–1255. Kyoto, Japan (2010). http://accelconf.web.cern.ch/AccelConf/IPAC10/papers/tuymh02.pdf.

[8] Calvey, J. R., *et al.* *CesrTA Retarding Field Analyzer Measurements in Drifts, Dipoles, Quadrupoles and Wigglers.* pages 1970–1972 (2010).

[9] Tomassini, S., *et al.* *A New RF Shielded Bellows for DAΦNE Upgrade.* Eleventh European Particle Accelerator Conference Proceedings, pages 1706–1708 (2008).

[10] ERL@CESR. *Project Execution Plan* (2011). To Be Completed.

[11] ARUP. *Energy Recovery Project Definition Design, Volume I Report.* Technical report (2010).